

## Article

# A Framework for Adaptive Façade Optimization Design Based on Building Envelope Performance Characteristics

Ping Chen \*  and Hao Tang

School of Architecture and Urban Planning (SAU), Shandong Jianzhu University, Jinan 250101, China; 2021055236@stu.sdjzu.edu.cn

\* Correspondence: chenping543@sdjzu.edu.cn; Tel.: +86-186-6077-6468

**Abstract:** The adaptive façades serve as the interface between the indoor and outdoor energy of the building. Adaptive façade optimization design can improve daylighting performance, the thermal environment, view performance, and solar energy utilization efficiency, thus reducing building energy consumption. However, traditional design frameworks often neglect the influence of building envelope performance characteristics on adaptive façade optimization design. This paper aims to reveal the potential functional relationship between building façade performance characteristics and adaptive façade design. It proposes an adaptive façade optimization design framework based on building envelope performance characteristics. The method was then applied to a typical office building in northern China. This framework utilizes a K-means clustering algorithm to analyze building envelope performance characteristics, establish a link to adaptive façade design, and use the optimization algorithm and machine learning to make multi-objective optimization predictions. Finally, Pearson's correlation analysis and visual decision tools were employed to explore the optimization potential of adaptive façades concerning indoor daylighting performance, view performance, and solar energy utilization. The results showed that the optimized adaptive façade design enhances useful daylight illuminance (UDI) by 0.52%, quality of view (QV) by 5.36%, and beneficial solar radiation energy (BSR) by 14.93% compared to traditional blinds. In addition, each office unit can generate 309.94 KWh of photovoltaic power per year using photovoltaic shading systems. The framework provides new perspectives and methods for adaptive façade optimization design, which helps to achieve multiple performance objectives for buildings.

**Keywords:** adaptive façades; building envelope performance; daylighting performance; quality of view; solar energy utilization; K-means clustering algorithm; multi-objective optimization



**Citation:** Chen, P.; Tang, H. A Framework for Adaptive Façade Optimization Design Based on Building Envelope Performance Characteristics. *Buildings* **2024**, *14*, 2646. <https://doi.org/10.3390/buildings14092646>

Academic Editor: Apple L.S. Chan

Received: 3 July 2024

Revised: 11 August 2024

Accepted: 22 August 2024

Published: 26 August 2024



**Copyright:** © 2024 by the authors. Licensee MDPI, Basel, Switzerland. This article is an open access article distributed under the terms and conditions of the Creative Commons Attribution (CC BY) license (<https://creativecommons.org/licenses/by/4.0/>).

## 1. Introduction

Over the past three decades, as human demand has continued to grow, energy consumption in the building sector has shown a significant upward trend, with the building sector accounting for about 40% of global energy consumption [1]. At the 75th United Nations General Assembly, China pledged to peak its domestic carbon emissions by 2030 and to become carbon neutral by 2060. However, public buildings that excessively pursue large-area glass curtain walls often consume much energy to maintain a stable indoor environment [2]. As of 2023, the world's energy demand is growing at nearly 1.8% per year [3]. Therefore, performance simulation, prediction, and evaluation at the early building design stage have great potential for building energy conservation and emission reduction [4].

The building envelope and the building skin are two essential components of a building. They are the transition zones for exchanging material and energy between the interior and exterior. The building envelope is a significant barrier separating indoor and outdoor environments and effectively protects against adverse environmental influences. The building envelope significantly affects the visual and thermal comfort of users, as well as the building's energy consumption [5]. As a regulator of the building envelope, the building

skin can effectively regulate the outdoor environment's direct effect on the building envelope and plays a crucial role in improving the quality of the indoor environment [6]. Research shows that people spend 90% of their time indoors [7]. The indoor environment's quality, determined by factors such as the indoor daylight environment, thermal environment, and view performance, significantly impacts users' lives [8,9]. Several studies have emphasized balancing daylighting performance and view performance to create a comfortable indoor environment [10]. The synergistic effect of the building envelope and building skin is not only critical to building design in terms of functionality and aesthetics but also plays a vital role in improving building performance in terms of indoor daylighting, view performance, and solar energy utilization [11]. This study only considers the building envelope for the building façade structure.

Sunlight, as a direct source of natural daylight, can improve the indoor daylight environment and significantly enhance user productivity and efficiency [12]. However, the variability in the sky environment and the ever-changing angle of sunlight incidence can lead to an uneven distribution of indoor daylight and potential glare issues [13,14], resulting in problems such as visual fatigue and impairment, which can seriously impact the users' quality of life [15]. If lighting fixtures are provided for indoor areas with insufficient daylighting, not only will they increase building energy consumption but traditional lighting also lacks the spectral combination and quality required to stimulate the circadian rhythm system [16]. Therefore, when designing building skins, it is necessary to balance the indoor daylighting performance requirements with the potential risk of glare discomfort, improve the quality of indoor daylighting, and create a favorable indoor daylight environment.

As one of the essential functions of the building envelope, visual field observation establishes a visual connection with the external environment through windows, significantly impacting indoor users' physiological comfort and psychological health [17,18]. Having a good view can positively influence indoor users' physical and mental health [19], happiness [20], and comfort [21]; improve users' mood and spatial satisfaction; and thus increase work efficiency by 10–25% [22]. However, some dense building skin designs can disrupt the window view landscape, negatively affecting the users' physical and mental health [17]. Quality of view (QV) is an important indicator for evaluating indoor view performance. However, previous research on indoor environmental quality usually presented a subjective evaluation or directly ignored QV [17], resulting in limited relevant research methods and evaluation indicators [23,24]. Improvements were not made until the introduction of the LEED v4 standard by the Chartered Institution of Building Services Engineers (CIBSE) and the New European Daylighting Standard EN 17037 [25] into the design guidelines. Through performance simulation, the subjective judgment of QV is transformed into objective data indicators, which improve the reliability of research methods and evaluation indicators of view performance [26].

Solar energy is the most important renewable and clean energy source, which not only plays a crucial role in improving the indoor thermal environment but also holds significant importance in helping boost solar photovoltaic power generation and contributing to energy savings and emission reduction [27]. In the field of architecture, the utilization of solar energy is primarily divided into two categories: passive and active [28]. The building envelope, as the primary receiving surface of solar radiation, utilizes passive technology to regulate solar indoor entry, thereby improving the indoor thermal environment. Especially in cold climate regions, solar energy is a vital factor for enhancing the indoor thermal environment of the building [29]. The active utilization of solar energy, represented by photovoltaic power generation technology, has propelled the development of two types of buildings: building integration photovoltaic (BIPV) [30] and building attached photovoltaic (BAPV) systems [31]. Photovoltaic shading systems (PVSSs), one of the essential technical means for these two types of buildings, can regulate the indoor daylight environment and utilize solar photovoltaic power generation [32]. However, an excessive increase in the area of photovoltaic shading panels can harm the indoor daylight environment, impairing the quality of the users' view and reducing indoor comfort. Therefore, when

utilizing solar radiation energy to improve the indoor thermal environment, it is necessary to fully consider other building performance objectives, such as indoor daylighting performance and view performance, and design the PVSSs reasonably to achieve the goal of sustainable development.

In summary, the interaction between the building envelope and building skin has significant impacts on the quality of the indoor environment, solar energy utilization, and sustainability. However, multiple building performance objectives need to be considered when optimizing the design of the building skin. The relationship between these performance objectives is not simply linear; there may even be contradictory relationships that constrain each other. Therefore, this paper proposes a method of adaptive façade design based on the performance characteristics of the building envelope to solve these contradictions. The potential functional connections between building envelope performance characteristics and adaptive façade design were explored by integrating four performance objectives to achieve a good indoor environment and efficient solar energy utilization.

## 2. Background

As the primary type of outdoor shading for buildings, building skins are investigated for their shape, material, size, and motion adjustment methods to explore their potential performance in improving indoor daylighting performance, view performance, and solar energy utilization efficiency [33,34]. However, most existing research focuses on single performance studies, such as daylighting performance or energy consumption, with relatively few comprehensive analyses covering the three dimensions of the indoor daylight environment, thermal environment, and solar energy utilization. There are considerably less studies on the analysis of indoor viewing performance. Secondly, the adaptive façade proposed by Loonen et al. [35] has been widely favored by architects due to its flexible and changeable structural attributes, demonstrating significant advantages in responding to changes in climatic environments, user preferences, building performance, and the aesthetics of building façades [36]. This flexible form and multiple functional requirements place higher demands on design methods and efficiency. Additionally, previous studies have often used horizontal grid sensor indicators to directly explain the impact of building skin on indoor performance [24,37], ignoring the direct connection between building envelope performance characteristics and the building skin.

Traditional blinds, one of the most common building skin types, primarily improve indoor daylighting performance by shading sunlight directly with a single performance objective. However, the design of blinds with a fixed tilt angle may lead to poor daylighting performance and potentially increase the energy consumption of the building [38]. Olbina et al. [39] pointed out that different parts of the window carry multiple functions, requiring different skin forms and control strategies in different parts of the window. The emergence of a split blind system solves this problem, dividing traditional blinds vertically into three parts and providing 400–500 Lux daylight illumination in 45% of the wintertime by controlling the angle of the slats in different parts to meet different functional requirements, saving 12% to 37% of the annual electrical lighting energy consumption. In order to effectively solve the problem of uneven indoor daylighting and reduce the influence of glare, Alsukkar et al. [40] modified the split blind system. Blinds were divided into upper and lower parts based on the dual functions of building envelope daylight and shading heat protection, which successfully solved the problem of indoor glare and increased the uniformity of indoor daylighting performance to 60%, significantly improving the quality and comfort of indoor daylighting. Subsequently, a light shelf was installed into the split blind system. By adjusting the spacing and angle of the light shelf, more sunlight was reflected into the deep indoor space, improving the deep indoor space daylight environment and providing a guide for adjusting the rotational angle of the blinds in response to regular changes in the split blinds' control [41]. Furthermore, to reduce the effect of blinds on the indoor view performance, Kim et al. [42] not only improved the indoor daylighting performance but also ensured a satisfactory view performance by controlling the projection

length and tilt angle of the blind slats. Valitabar et al. [43] proposed a multi-layer blind system (MLBS) consisting of seven groups of three separated slats, which can rotate around a horizontal axis. The middle slats are marked as visual field blinds to control daylighting performance and view performance. The combination of the MLBS and a light shelf offers a practically glare-free indoor space. Most studies improve building performance by controlling the width or rotation angle of blinds, but the single-function blind has some limitations in performance improvement. Although a few studies have considered the combination design of different types of building skins, there is also a lack of data support for building skin combination design.

With the development of parametric and performance simulation techniques [44], the building skin has been transformed from a static monomorphic form to an adaptive façade. Research has been gradually focused on the potential connection between the building envelope's performance characteristics and the adaptive façade's design, aiming for a design more responsive to changes in the external environment and the users' needs. Kim et al. [45–47] proposed a design strategy for the adaptive façade based on the parametric behavior diagram (PBM). This strategy determines the most suitable adaptive façade state for the outdoor environment every hour by collecting the amount of solar radiation received by the adaptive façade in different states each hour. It integrates the optimized adaptive façade state into the entire building envelope to improve the indoor daylight environment and reduce energy consumption. Furthermore, Samadi et al. [48] controlled the rotation angle of each adaptive façade unit using data from the incident angle of sunlight and the daylighting test points on the ceiling, achieving precise regulation of indoor daylighting performance. Wang et al. [49] utilized performance simulation technology to analyze the solar radiation intensity on the building envelope. The adaptive façade was specifically designed based on differences in solar radiation distribution, resulting in a 14.8% improvement in indoor thermal comfort with the air conditioning on and a 4.7% improvement with the air conditioning off. Moreover, the building's energy consumption was reduced by 20%. Despite the overall improvement in the building's performance in this study, the use of a 3 m × 3 m grid division in the analysis of solar radiation intensity led to some building units having adaptive façade distributions that were too compact. Consequently, Wang et al. [50] divided the envelope between the two columns into three smaller regions in the simulation platform. They selected the simulated average of the solar radiation at the center of each area as the basis for designing the adaptive façade, resulting in improved solar radiation heat gain and indoor daylighting performance. In addition, Shen et al. [51] designed the adaptive façade into different module units, calculated the daylight coefficients of each module unit, and finally achieved the optimal design of the adaptive façade through integer programming. Meanwhile, Hosseini et al. [52–54] established a connection between users and the sun's position through a simulation platform. They used the intersection point of this line with the building envelope as the attracting point for adaptive façade control, thus achieving user-centered adaptive façade design. Multiple variable factors influence the optimization of adaptive façade design and require weighing several performance objectives. The complexity mentioned above increases the time and cost of performance simulation calculations.

Since 2010, artificial intelligence (AI) technologies have been progressively used in all phases of the building lifecycle to improve building sustainability and building energy efficiency [55–57]. In particular, AI technologies and optimization algorithms have been introduced into the building design process to provide new ideas and methods for building design. AI technologies can quickly process the hidden relationships between various data and make accurate predictions, and with the fast search capability of optimization algorithms, they can explore multiple possibilities of design and find the optimal design solution. Initially, an artificial neural network was utilized to investigate the relationship between the blind slat angle and indoor daylighting, which enhanced building skin design efficiency [58]. Subsequently, Gadelhak et al. [59] integrated a building performance simulation and optimization algorithms. They used a genetic optimization algorithm to

enhance indoor daylighting by combining light shelves and vertical blinds. This method resulted in multi-objective performance optimization in the design of the adaptive façade. Sadegh et al. [60] used a multi-objective optimization method to explore the influence of factors such as the distance between the adaptive façade and the building envelope, the size of the adaptive façade unit, and how the adaptive façade is adjusted on indoor daylighting performance. This strategy resolved the mutual contradictions between the parameters at the early design stage, resulting in improved office building daylighting performance. Luo et al. [61] utilized radial basis function neural networks to predict the influence of the adaptive façade on indoor daylighting performance. Lin et al. [62] explored the internal relationship between different adaptive façade forms and building performance. They used daylight penetration as the “intermediate characteristic value” between parameters and objectives, training a neural network model for daylighting performance capable of predicting the adaptive façade of various building types. El-Mowafy et al. [63] investigated the environmental response capacities of different adaptive facades. They extracted 22 variables, defined 18 adaptive façade models, and utilized the K-nearest neighbor algorithm to find the optimal shading system, thus improving building performance. Li et al. [64] explored the impacts of different adaptive façades on building daylighting performance through machine learning. Additionally, Alsharif et al. [65] combined machine learning with multi-objective optimization algorithms to determine the optimal size and rotation angle for adaptive façade design, minimizing thermal discomfort time, energy consumption, and total shading area. The combination of these advanced technologies offers more architectural design possibilities and significantly improves the quality and efficiency of design.

In summary, the existing research and application of adaptive façade optimization design face three main limitations or deficiencies. These are as follows:

1. Existing research primarily focuses on enhancing indoor daylighting or thermal environments by controlling the geometric dimensions and rotation angles of adaptive façades, with only a few studies exploring the indoor view performance. However, research has yet to be conducted that integrates and analyzes the four performance objectives of indoor daylighting, view performance, solar radiation heat gain, and solar photovoltaic power generation in buildings.
2. There is a close connection and interaction between the building envelope and the adaptive façade, and adjusting the adaptive façade to change the direct influence of the external environment on the building envelope improves numerous building performances. However, existing research usually establishes a direct link between adaptive façade design parameters and building performance objectives, neglecting the direct influence of building envelope performance characteristics on adaptive façade design. As a consequence, adaptive façade designs lack precision and relevance.
3. Traditional static and single-form building skins cannot meet indoor daylighting, thermal environment, and user needs simultaneously. In contrast, adaptive façades respond to external environmental changes by adjusting various design parameters to enhance multiple aspects of building performance. However, traditional design methods struggle with solving problems involving multiple objectives and parameters.

This study explores the potential of adaptive façades for multi-objective performance optimization in office buildings. The novelty presents an adaptive façade optimization design framework based on building envelope performance characteristics. At the early design stage, the building envelope’s performance characteristics are analyzed and divided into parts with different functional attributes. Based on the division results, the design of the building’s adaptive façade modular units is guided. The framework integrates the analysis of multi-objective building performance to create good indoor daylighting and thermal environments while ensuring indoor view performance, improving the efficiency of solar photovoltaic power generation, and reducing the building’s energy consumption.

### 3. Methods

This section proposes an adaptive façade optimization design framework based on building envelope performance characteristics. The framework consists of five main steps:

1. Create office parametric and performance models;
2. Analysis of building envelope performance characteristics;
3. Adaptive façade modular unit design;
4. Training neural network prediction models;
5. Multi-objective optimization and decision-making.

Figure 1 illustrates the framework for integrating 3D parametric models, performance models, neural network prediction models, and multi-objective optimization decisions using Rhinoceros 7.0 and Grasshopper software [66]. The performance characteristics of the building envelope were analyzed by a clustering algorithm, and based on the clustering analysis results, adaptive façade modular units with different functions were designed in a targeted manner. Decision-making for the optimal adaptive façade solution for office space was performed in terms of indoor daylighting performance, view performance, solar radiation heat gain, and solar photovoltaic power generation. The research used a personal computer (Intel Core i7 2.80 GHz and 16 GB RAM) for development and experimentation.

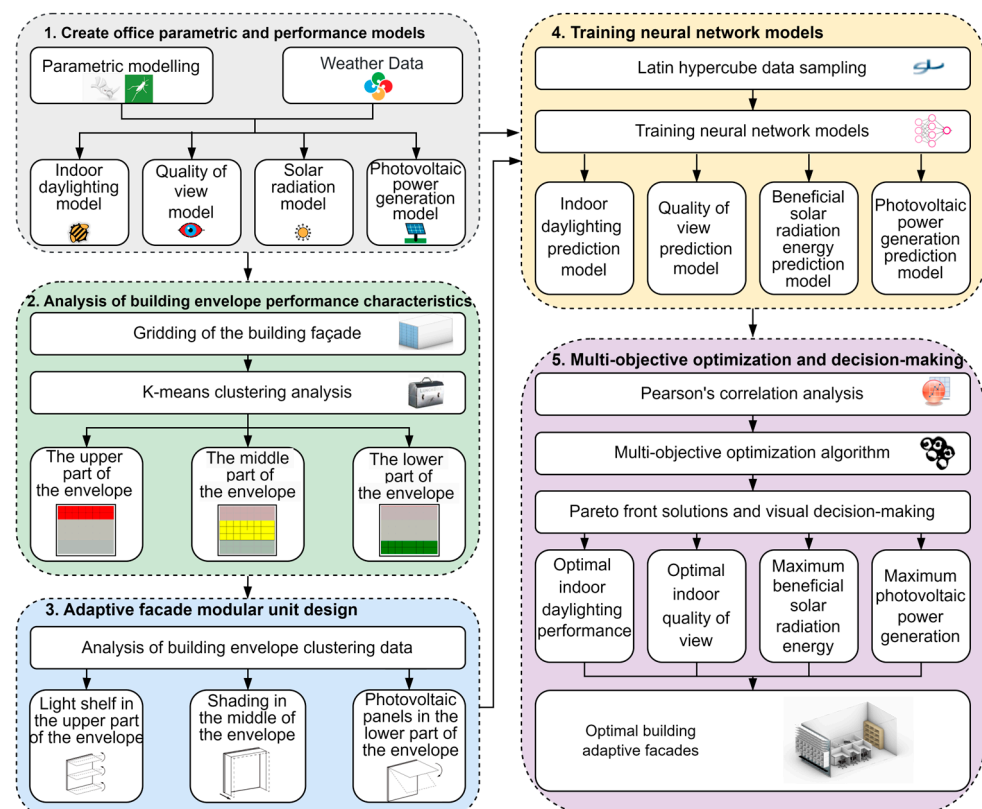


**Figure 1.** Integrated 3D parametric model, performance model, neural network prediction model, and multi-objective optimization and decision-making workflow.

#### 3.1. Create Office Parametric and Performance Models

The study was conducted in Jinan, a city in northern China located at  $36^{\circ}40'$  N and  $117^{\circ}00'$  E. The city belongs to warm temperate semi-humid monsoon climate with hot, rainy summers and cold, dry winters [67]. With the influence of solar radiation, general atmospheric circulation, and the geographical environment, the peak dry-bulb temperature in Jinan is as high as  $42^{\circ}\text{C}$ , and the coldest temperature in winter is around  $-19^{\circ}\text{C}$ . This results in global horizontal irradiance, in particular, direct normal irradiance, mostly from the south. Therefore, when designing adaptive façades for buildings, it is necessary to

weigh multiple performance objectives, such as warmth in winter and coolness in summer. A typical office building in the city of Jinan, facing south, was selected as a case study. The mid-floor office unit of the building was selected for parametric modeling, with spatial dimensions of  $4.2\text{ m} \times 7.2\text{ m} \times 3.6\text{ m}$  and a window-to-wall ratio of 0.95 (Figure 2). The open-source Ladybug tools provided by the Grasshopper platform were used to construct the indoor daylighting model, the quality of view model, the solar radiation model, and the photovoltaic power generation model, respectively. Ladybug tools are proven simulation tools that have been widely used [68,69]. The workflow utilizes EnergyPlus Weather Data meteorological data provided by the U.S. Department of Energy.

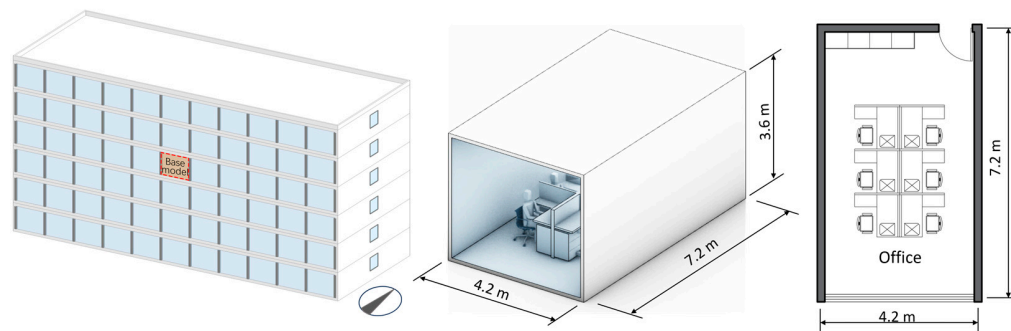


**Figure 2.** Example of an office unit plan and 3D model.

### 3.1.1. Indoor Daylighting Model

The primary indicators for evaluating indoor daylighting include the daylight factor (DF) [70], daylight coefficient (DC) [71], useful daylight illuminance (UDI) [72], and daylight autonomy (DA) [73]. Since DF and DC are commonly used evaluation metrics for a static daylighting analysis, their use in a dynamic daylighting evaluation may lead to inaccurate calculations. Therefore, UDI is selected as the evaluation index for an indoor dynamic daylighting environment. UDI is divided into three evaluation levels based on the illuminance range: less than 100 Lux, 100–2000 Lux, and over 2000 Lux. The illuminance value between 100 Lux and 2000 Lux is indicated to ensure the demand for indoor daylighting while also avoiding the hazards of glare or overheating indoors caused by excessive sunlight. Honeybee utilized Daysim and Radiance tools to conduct an hour-by-hour daylighting simulation analysis throughout the year. The measurement grid size was set at  $0.5 \times 0.5\text{ m}$ , located at a height of 0.8 m above the office desktop, with a total of 112 daylighting test points. The reflectance (R) of the office building boundary materials is listed in Tables 1 and 2 shows the radiance simulation accuracy settings.

**Table 1.** Setting of boundary condition reflectance (R) values.

Boundary Conditions	Reflectance
Floor	0.30
Ground	0.50
Ceiling	0.85
Window	0.80

**Table 2.** Simulation accuracy settings for radiance.

Radiance Parameters	Ambient Bounces	Ambient Divisions	Ambient Sampling	Ambient Accuracy	Ambient Resolution
Medium Quality	4	1024	256	0.2	64

### 3.1.2. Quality of View Model

A quality of view (QV) assessment, according to the green building standard LEED v4 [74], requires that at least 75% of the commonly used building area be directly connected

to the outdoor landscape through vision glazing. Furthermore, at least two of the following four landscapes must be satisfied: (a) multiple lines of sight separated by at least 90 degrees in different directions from the vision glazing; (b) include outdoor natural landscape or urban landscape elements; (c) unobstructed view fields are within three times the height of the head of the vision glazing; and (d) have a view factor of at least greater than 3. Ladybug tools was used to analyze QV, and a 60-degree horizontal cone was selected as human vision to study the range of visual fields from the indoor space to the outdoor landscape. The simulation principle involves emitting radiation 360 degrees around each viewpoint based on the horizontal line of the field of view within a 60-degree cone range. The number of lines of sight passing through the window is counted, and the percentage of the field of view for each test point is calculated. The indoor area percentage that meets the field of view quality requirements is selected based on the field of view factors. The QV test grid is located at a height of 1.2 m from the ground when office workers are sitting. The measurement grid size is set to 0.3 m × 0.3 m, totaling 336 test points.

### 3.1.3. Solar Radiation Model

Solar radiation has a significant impact on the indoor thermal environment. Windows, as one of the most essential components of the building envelope, are characterized by low thermal resistance and high thermal conductivity. Therefore, in order to prevent indoor overheating during the hot summer months, the direct connection between solar radiation and the room should be reduced. In order to increase indoor temperatures during the cold winter months, it is necessary to increase the amount of indoor solar radiation. Designers should thoroughly consider the impact of solar radiation on the indoor thermal environment of buildings during both winter and summer [75,76] to maximize the utilization of solar radiation energy. The environmental analysis module of Ladybug tools created the solar radiation model. The window was used as the test surface, and the grid size was set to 0.3 × 0.3 m, totaling 143 test points. The solar radiation energy for winter (December–February) and summer (June–August) was calculated separately. The beneficial solar radiation energy (BSR) was determined by subtracting the harmful solar radiation energy in the summer from the solar radiation energy in the winter. The equation is as follows:

$$BSR = TSR_{winter} - TSR_{summer} \quad (1)$$

where *BSR* represents beneficial solar radiation energy, *TSR<sub>winter</sub>* represents winter solar radiation energy, and *TSR<sub>summer</sub>* represents summer solar radiation energy.

### 3.1.4. Photovoltaic Power Generation Model

Solar energy primarily exists in the form of sunlight and thermal radiation. The heat from solar radiation can directly enhance the indoor thermal environment, meeting users' needs for indoor comfort. Sunlight provides sufficient daylight for the room and improves the quality of indoor daylighting. It can also be converted into renewable energy through photovoltaic power generation technology to use clean energy efficiently. The renewable energy module of Ladybug tools was employed to construct a solar photovoltaic power generation model. Polysilicon, with a photovoltaic conversion efficiency of 15.42%, was selected as the photovoltaic material to calculate the photovoltaic power generation (PVG) for one year. The settings of the above performance model remained consistent throughout the workflow.

## 3.2. Analysis of Building Envelope Performance Characteristics

As mentioned above, the building envelope's primary performance characteristics include daylighting, thermal, and indoor view performance. The study identified three key indicators to represent these performance characteristics: UDI, QV, and BSR. Firstly, the building envelope was divided into multiple unit modules to assess these performance characteristics. Subsequently, the performance simulation of each unit module was carried out individually. The performance indicator values of each unit module were collected,



and the data were analyzed using the K-means clustering algorithm to divide the building envelope into parts with different functional attributes.

When analyzing the performance characteristics of the building envelope, it is necessary to ensure the precision of the division of the functional attributes of the building envelope and to consider the dimensional design of the adaptive modular units. Based on the parametric model created in Section 3.1, the building envelope was divided into 56 individual unit module windows, each measuring  $0.5 \times 0.5$  m. Each unit module window was assigned a serial number ranging from 0 to 55. The three building performance models from Sections 3.1.1–3.1.3 were integrated, and the performance indicators UDI, QV, and BSR were simulated for each unit module window in turn. It is worth noting that during the simulation and analysis of the indoor view performance, the field of view factor needed to be set to 0 due to the small size of each unit module window. A field of view factor greater than 0 at a test point indicates that the window view is visible at that location; otherwise, it is not. To avoid the influence of data types of different dimensions and magnitudes on the clustering algorithm and to ensure consistency, the performance indicators of the simulation calculation were normalized. The results are shown in Figure 3, and the normalized equation is as follows:

$$x^* = \frac{x - x_{\min}}{x_{\max} - x_{\min}} \quad (2)$$

where  $x$  represents the original data,  $x_{\max}$  represents the maximum value in the set,  $x_{\min}$  represents the minimum value in the set, and  $x^*$  represents the normalized data.

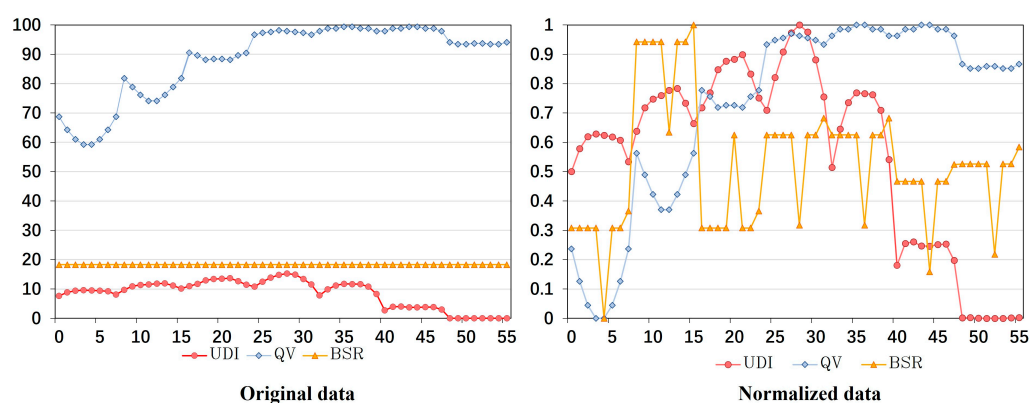


**Figure 3.** Original data (left panel) and normalized data (right panel) of unit module performance characteristics.

K-means is an unsupervised clustering algorithm that groups data objects with the same characteristics through similarity calculations among data objects. The algorithm has been widely used, with a fast clustering speed and a good clustering effect [77]. The algorithm divides the data into  $k$  clusters based on  $n$  given sets of data objects, each containing at least one data object, and each data object can only belong to one cluster. This study uses the K-means clustering algorithm to perform a cluster analysis of the normalized unit module performance characteristic values, with the  $K$  value set to 3. As depicted in Figure 4, the building envelope is segmented into three parts of the region—upper, middle, and lower—through cluster analysis.

### 3.3. Adaptive Façade Modular Unit Design

The purpose of Figure 5 is to further investigate the results of building envelope division and extract the performance characteristic values of each region unit module for a box diagram analysis. Firstly, the average size of the performance indicators UDI, QV, and BSR in the upper part of the building envelope is ranked as follows: UDI (0.658) > BSR (0.506) > QV (0.281). This ranking indicates that indoor daylighting and thermal performance are

the main functions of this part. When designing adaptive façades for this part, it is essential to focus on enhancing indoor daylighting and reducing the obstruction of solar radiation energy. Secondly, the average size of the performance indicators UDI, QV, and BSR in the middle part of the building envelope is ranked as follows: QV (0.893) > UDI (0.793) > BSR (0.488). This ranking indicates that the indoor view and daylighting performance are the main functions of this part. In designing the adaptive façade for this part, emphasis should be placed on reducing visual field obstructions and improving daylighting performance. Additionally, the average size of the performance indicators UDI, QV, and BSR for the lower part of the building envelope is ranked as follows: QV (0.920) > BSR (0.465) > UDI (0.119). This ranking indicates that the indoor view and thermal performance are the main functions of this part. When designing adaptive façades, focusing on reducing obstructions to the visual field and maximizing BSR is necessary. After a comprehensive analysis of the performance characteristic values of the upper, middle, and lower parts of the building envelope, it was found that the upper and middle parts significantly impact UDI. Furthermore, the building envelope's middle and lower parts significantly impact QV. The influence of BSR on the three parts of the building envelope is almost equivalent.

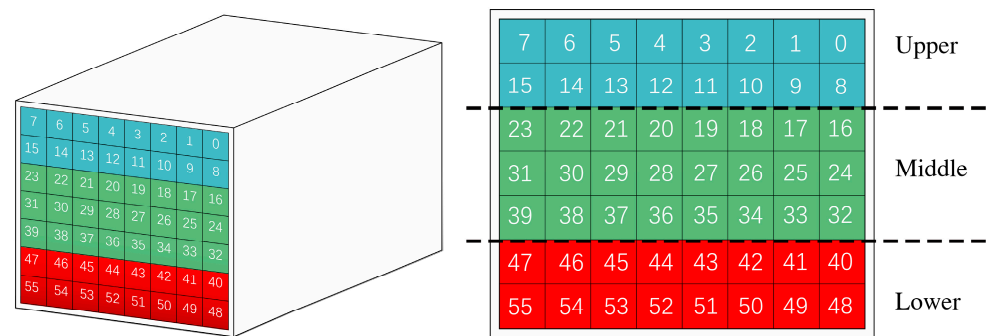


**Figure 4.** Clustering of building envelope performance characteristic values.

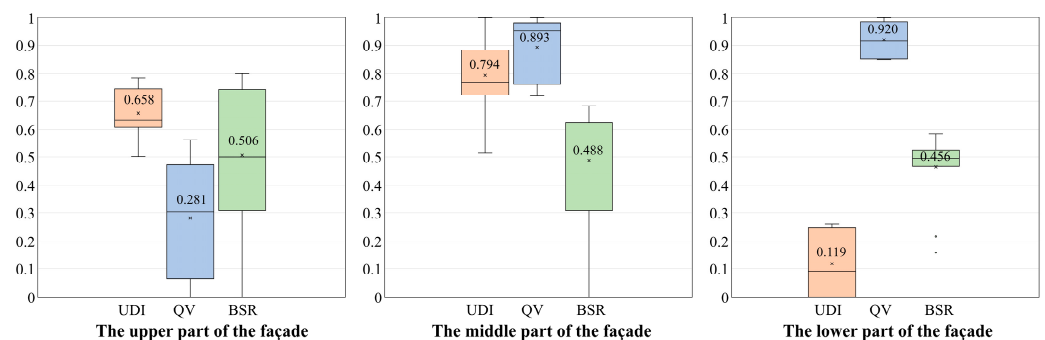


**Figure 5.** Analysis of the performance characteristic values of each part of the building envelope.

Based on the results of K-means clustering analysis of the performance characteristics of the building envelope, a highly integrated and multifunctional adaptive façade is designed, and parameterized adaptive façade modular units are designed for the upper, middle, and lower parts of the building envelope through the Grasshopper platform. The aim is to realize an immediate response to external environmental changes through the adjustment of each part of the adaptive modular unit so as to improve the overall performance of the building.

Firstly, for the upper part of the building envelope, it adopts light shelf devices to reflect more outdoor sunlight into the deep indoor space and utilizes its own shading to reduce the risk of glare near the windows, thus increasing the overall proportion of useful daylight illuminance in the room. The part improves the indoor daylighting environment by flexibly adjusting the width and angle of the modular units by applying the principles of translational change and horizontal rotation angle to different light shelf types. The design

parameters of the part therefore include the light shelf type (LST), light shelf width (LSW), and light shelf angle (LSA).

Secondly, based on the results of the performance characterization of the middle part of the building envelope, the focus of the design of this part of the adaptive façade modular unit is to reduce the obstruction of the visual field and maximize the use of daylighting. The design of this part of the adaptive façade focuses on arranging the three skin forms of vertical shading, horizontal shading, and comprehensive shading along the boundaries of the modular units and adopts the principle of translational change in order to regulate the width of the shading plates, which in turn improves the quality of the indoor view and controls the effect of indoor daylighting. Therefore, the design parameters of this part include the shading plate type (SPT) and shading plate width (SPW).

Finally, the study improves solar energy utilization to meet the functional requirements of the lower part of the building envelope while also ensuring indoor view performance. The study utilized a photovoltaic shading system (PVSS), which not only provides shading but also integrates photovoltaic power generation technology. This photovoltaic shading system is capable of adjusting the width and angle of the photovoltaic shading plate according to the change in solar orientation through the principles of translational change and rotational change to ensure that the photovoltaic shading plate has a maximized photovoltaic energy production area, thus increasing the photovoltaic power generation benefits of the building envelope. Therefore, the design parameters of this part include the photovoltaic shading width (PVW) and photovoltaic shading angle (PVA). Table 3 shows the form of the adaptive façade module units, and Table 4 shows the design parameter constraints and range of material settings.

**Table 3.** Adaptive façade modular unit forms.

Module Unit Type	I	II	III	IV
Light Shelf (Upper part of the envelope)				
Shading Plate (Middle part of the envelope)				
Photovoltaic shading (Lower part of the envelope)				

**Table 4.** Module units' design parameter constraint ranges and material reflectance (R).

Parameter Variables	Min	Max	Steps	Unit	Reflectance
Light Shelf Type	1	4	1	-	
Light Shelf Width	0.0	0.9	0.1	m	0.84
Light Shelf Angle	0	90	10	degree	
Shading Plate Type	0	2	1	-	
Shading Plate Width	0.0	0.9	0.1	m	0.30
Photovoltaic Shading Width	0.0	0.6	0.1	m	
Photovoltaic Shading Angle	0	90	10	degree	0.35

### 3.4. Training Neural Network Prediction Models

The performance simulation process takes too long due to the complexity and diversity of design parameters and optimization objectives. Utilizing artificial neural networks to establish a mapping model between adaptive façade design parameters and performance objectives allows for rapid building performance prediction. This study employed the Grasshopper platform to build backpropagation neural network (BPNN) prediction models using the LunchBox tool [78]. These models include an indoor useful daylighting illuminance backpropagation neural network prediction model (BPNN\_UDI), an indoor quality of view backpropagation neural network prediction model (BPNN\_QV), a beneficial solar radiation energy backpropagation neural network prediction model (BPNN\_BSR), and a photovoltaic power generation backpropagation neural network prediction model (BPNN\_PVG). Training these neural network prediction models consists of three steps: gathering sample data, optimizing neural network hyperparameters, and validating neural network prediction models accurately.

#### 3.4.1. Gathering Sample Data

The study uses Latin Hypercube Sampling (LHS) [79] to improve the simulation efficiency and optimize the adaptive façade design process. LHS randomly selects a specified number of feasible solution samples from the diverse set of adaptive façade design parameters. Subsequently, the optimization objectives corresponding to these samples are simulated and calculated using performance models. These calculated values serve as the sample data for the training prediction model. The sample data are divided into training and validation datasets for neural network training and validation. Previous research has shown that samples larger than twice the number of design parameters provide a better representation of architectural design space [80]. In order to improve the accuracy of the prediction model as much as possible, the number of samples was set to 400, and the sampling process was completed within the Simlab 2.2 software, which represented adaptive façade design solutions with different characteristics. The sampled design parameters were then loaded into Grasshopper's Panel module as input data for the prediction model. The four building performance objectives of UDI, QV, BSR, and PVG were simulated separately in conjunction with the performance model in Section 3.1, and the calculated performance data were used as the output data for training the prediction model.

#### 3.4.2. Optimizing Neural Network Hyperparameters

Before the neural network hyperparameter optimization, preprocessing of the adaptive façade design parameters and building performance objective data is required, which includes data normalization and division into a training set and a validation set. Firstly, the design parameters and performance objective data need to be normalized, and all input values were normalized from 0 to 1 along the feature axis. Secondly, 400 sets of data were divided into a training dataset and a validation dataset at a ratio of 8:2, with 320 sets of data used to train the BPNN model and 80 sets of data used to validate the prediction accuracy of the BPNN model.

Optimizing the BPNN model's hyperparameters is required to enhance the model's prediction accuracy. The hyperparameters of the BPNN model include the number of hidden layer layers, the number of neurons in the hidden layer, and the learning rate, which directly determine the prediction accuracy of the BPNN model and do not change with the number of training times. A complex, black-box relationship exists between hyperparameters and prediction model accuracy, making it challenging to debug various parameters manually. Therefore, the SPEA2 optimization algorithm was used in this study to optimize BPNN training hyperparameters automatically. During the model training process, the objective is to minimize the mean squared error (MSE) between predicted and simulated values while maximizing the coefficient of determination ( $R^2$ ) of the predicted and simulated results. These criteria serve as guidelines for the hyperparameter optimiza-

tion process of the BPNN, aiming to achieve higher prediction accuracy. The calculation formulas for MSE and  $R^2$  are as follows:

$$MSE = \frac{1}{n} \sum_{i=1}^n (y_i - \hat{y}_i)^2 \quad (3)$$

$$R^2 = 1 - \frac{\sum_{i=1}^n (y_i - \hat{y}_i)^2}{\sum_{i=1}^n (y_i - \bar{y})^2} \quad (4)$$

where  $y_i$ ,  $\hat{y}_i$ , and  $\bar{y}$  denote the simulated value, the predicted value, and the average of the simulated values for the  $i$ -th sample, respectively, and  $n$  is the total number of samples.

### 3.4.3. Validating Neural Network Prediction Models Accurately

According to the  $R^2$  and MSE of the predicted value of the BPNN model and the simulated value, it was determined whether the predictive model could accurately reflect the mapping relationship between the adaptive façade design parameters and the building performance objectives.  $R^2$  signifies the proportion of the simulated values that can be explained by the predicted values, reflecting the degree of fit between the predicted and simulated values. A higher absolute value of  $R^2$ , closer to 1, indicates a better fit. Generally, when the  $R^2$  is higher than 0.93, the predicted values output from the BPNN model are considered to fit well with the simulated values. The MSE represents the error between the predicted and simulated values, with a smaller value indicating a more accurate description of the mapping relationship. The validation results of the four performance prediction models, as depicted in Figure 6, show that the MSE and  $R^2$  for each model meet the accuracy requirements, rendering them suitable for performance prediction. The hyperparameter settings of each prediction model are detailed in Table 5.

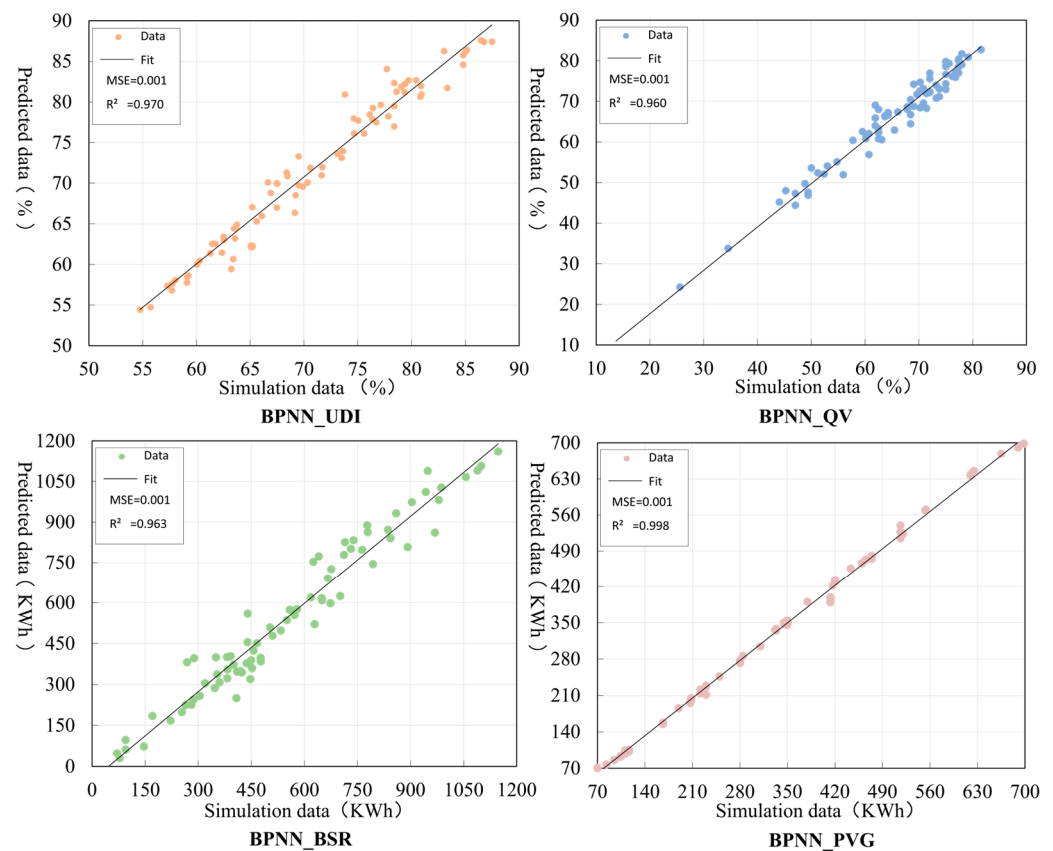


**Figure 6.** Accuracy validation of the four performance neural network prediction models.

**Table 5.** Neural network model hyperparameter settings and evaluation metrics.

Title	BPNN_UDI	BPNN_QV	BPNN_BSR	BPNN_PVG
Hidden Neurons	17	18	26	34
Learning Algorithm	Backpropagation	Backpropagation	Backpropagation	Backpropagation
Alpha	1.6	1.3	0.2	0.7
Activation Function	Sigmoid	Sigmoid	Sigmoid	Sigmoid
Iterations	2081	2412	2424	2340
Learning Rate	0.24	0.5	0.4	0.65
MSE	0.001	0.001	0.001	0.001
R2	0.970	0.960	0.963	0.998

### 3.5. Multi-Objective Optimization and Decision-Making

In order to determine the adaptive façade optimization design strategy, this study coupled the performance prediction model with the multi-objective genetic optimization algorithm, optimized and analyzed the design parameters of adaptive façade modular units in each part, obtained Pareto front solutions, and visualized the decision-making process by combining it with the Design Explorer platform [81]. The study selected Octopus, a plugin for the Grasshopper platform, to carry out multi-objective optimization [82], which performs optimization searches for multiple performance objectives through a genetic algorithm. According to the relevant literature and the experience of many experiments [76,83], the multi-objective genetic optimization algorithm is set up as described in Table 6. The Pareto front solution sets are obtained through the optimization algorithm and imported into the Design Explorer decision-making platform, where the screening criteria are set for each performance indicator. The optimal solution that meets the requirements is finally selected. This study aims to achieve the best four building performances of UDI, QV, BSR, and PVG through a multi-objective optimization algorithm. The objective functions are as follows:

$$f_1(LST_j, LSW_j, LSA_j, SPT_j, SPW_j, PVW_j, PVA_j) = \min(-UDI) \quad (5)$$

$$f_2(LST_j, LSW_j, LSA_j, SPT_j, SPW_j, PVW_j, PVA_j) = \min(-QV) \quad (6)$$

$$f_3(LST_j, LSW_j, LSA_j, SPT_j, SPW_j, PVW_j, PVA_j) = \min(-BSR) \quad (7)$$

$$f_4(LST_j, LSW_j, LSA_j, SPT_j, SPW_j, PVW_j, PVA_j) = \min(-PVG) \quad (8)$$

$$\min F(LST_j, LSW_j, LSA_j, SPT_j, SPW_j, PVW_j, PVA_j) = \min(f_1, f_2, f_3, f_4) \quad (9)$$

$$\text{s.t.} \begin{cases} LST_j \in [1, 2, 3, 4], \\ LSW_j \in [0.1, 0.2, 0.3, 0.4, 0.5, 0.6, 0.7, 0.8, 0.9], \\ LSA_j \in [0, 10, 20, 30, 40, 50, 60, 70, 80, 90], \\ SPT_j \in [1, 2, 3], \\ SPW_j \in [0.1, 0.2, 0.3, 0.4, 0.5, 0.6, 0.7, 0.8, 0.9], \\ PVW_j \in [0.1, 0.2, 0.3, 0.4, 0.5], \\ PVA_j \in [0, 10, 20, 30, 40, 50, 60, 70, 80, 90], \end{cases} \quad (10)$$

where  $f_1$ ,  $f_2$ ,  $f_3$ , and  $f_4$  are the four optimization objective functions.  $j$  is the number of design parameters.  $LST_j$ ,  $LSW_j$ ,  $LSA_j$ ,  $SPT_j$ ,  $SPW_j$ ,  $PVW_j$ , and  $PVA_j$  represent the light shelf type, the light shelf width, the light shelf angle, the shading plate type, the shading plate width, the photovoltaic shading width, and the photovoltaic shading angle, respectively, of the design parameters.

**Table 6.** The genetic optimization algorithm settings.

Boundary Conditions	Elitism	Mut. Probability	Mutation Rate	Crossover Rate	Population Size
Values	0.5	0.1	0.5	0.8	100

#### 4. Results

This section determines the potential relationship between adaptive façade design parameters and performance objectives through Pearson’s correlation analysis and a distribution plot of the design parameters for the Pareto front solutions to capture the data distribution characteristics quickly.

The 400 datasets sampled in Section 3.4 were imported into OriginPro2023b software for data analysis. The study plotted the seven adaptive façade design parameters and four performance objectives in a bivariate scatter matrix to test the linear correlation between them, as depicted on the left side of Figure 7. This result shows that a significant linear correlation exists between the performance objectives and multiple design parameters. As shown on the right side of Figure 7, the Pearson method was used for the correlation analysis between design parameters and performance objectives. The potential relationships between the adaptive façade design parameters and the four performance objectives of UDI, QV, BSR, and PVG were further explored. The Pearson correlation coefficient is between  $-1$  and  $+1$ . When the correlation coefficient is between  $-1$  and  $0$ , it indicates a negative correlation between the variables; when it is between  $0$  and  $1$ , it means a positive correlation. The larger the absolute value of the Pearson correlation coefficient, the stronger the correlation.

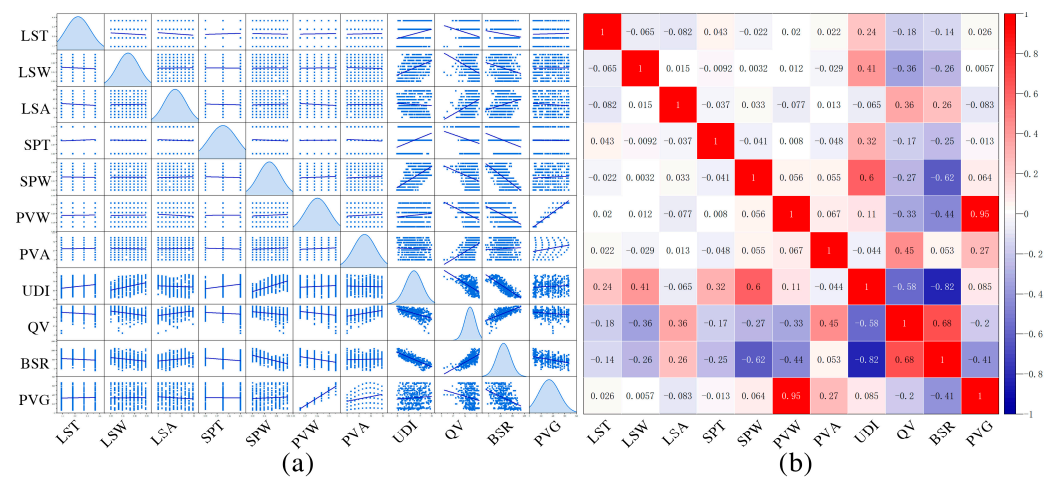


**Figure 7.** Bivariate scatter matrix (a) and Pearson’s correlation coefficient matrix (b).

As illustrated in Figure 7, the correlations between UDI and LST, LSW, and LSA are 0.24, 0.41, and  $-0.065$ , respectively. This suggests that indoor daylighting performance is primarily affected by LSW and has a weak connection with LST and LSA. The correlation coefficient between UDI and SPT is 0.32, indicating a moderate correlation between indoor daylighting performance and the SPT, and the correlation coefficient with SPW is 0.6, indicating that the changes in the SPW have a strong positive correlation with indoor daylighting performance. According to the correlation coefficients of UDI with PVW and PVA, which are 0.11 and  $-0.044$ , respectively, these design parameters have little to no effect on indoor daylighting performance.

Secondly, regarding the correlation analysis between the adaptive façade design parameters and the indoor view performance, the correlations between QV and LST, LSW, and LSA are  $-0.18$ ,  $-0.36$ , and 0.36, respectively, with LSW and LSA showing a moderately correlated relationship with the indoor view performance. LST has little effect on the indoor view performance. The correlation coefficients of QV with SPT and SPW are  $-0.17$  and  $-0.27$ , respectively, indicating that the SPT and the changes in the SPW have little effect on the indoor view performance. The correlation coefficients of QV with PVW and PVA are  $-0.33$  and 0.45, respectively, indicating that changes in PVW and PVA significantly affect the indoor view performance.

In the correlation analysis between adaptive façade design parameters and BSR, the correlation coefficients between the BSR and LST, LSW, and LSA are  $-0.14$ ,  $-0.26$ , and  $0.26$ , respectively. This suggests that LST, LSW, and LSA have only tiny impacts on BSR. Similarly, the correlation coefficients of BSR with SPT and SPW are  $-0.25$  and  $-0.62$ , respectively, which all show negative correlations. Notably, the SPW exhibits a strong negative correlation with the BSR, indicating that the changes in the SPW have a more significant impact. Furthermore, the correlation coefficient between BSR and PVW is  $-0.44$ , indicating that PVW significantly impacts BSR. The correlation coefficient with PVA is  $0.053$ , with only a marginal impact of changes in the degree of PVA on BSR.

Additionally, regarding the correlation analysis between PVG and adaptive façade design parameters, PVG's correlation coefficients with LST, LSW, and LSA are  $0.026$ ,  $0.0057$ , and  $-0.083$ , demonstrating that the light shelf has minimal impact on PVG. Additionally, the correlation coefficients of PVG with SPT and SPW are  $-0.013$  and  $-0.064$ , respectively, indicating that the shading plate has almost no effect on the PVG. The correlation coefficients of PVG with PVW and PVA are  $0.95$  and  $0.27$ , respectively, suggesting that the variation in PVW has a more significant impact on PVG than changes in PVA. In summary, LSW and SPW have more significant impacts on indoor daylighting performance and are positively correlated. PVD has a more significant impact on the indoor view performance, SPW has a more significant impact on BSR, and PVW has a more significant impact on solar photovoltaic power generation.

Lastly, Pearson's correlation coefficient was employed in this study to examine the potential relationships among the four performance objectives. The correlation coefficients of UDI with QV, BSR, and PVG are  $-0.58$ ,  $-0.82$ , and  $-0.085$ , respectively. UDI exhibits a strong negative correlation with QV and BSR, significantly impacting indoor daylighting performance. Furthermore, the correlation coefficients of QV with BSR and PVG are  $0.68$  and  $-0.2$ , respectively, indicating that BSR significantly impacts the indoor view performance. Lastly, the correlation coefficient between BSR and PVG is  $-0.41$ . Moreover, the correlation coefficient between BSR and PVG is  $-0.41$ , suggesting a moderately negative correlation between these performance objectives.

Since some of the adaptive façade design parameter combinations result in substandard building performance, screening criteria were established for the four performance objectives to enhance the efficiency of finding the Pareto front solution using the multi-objective optimization algorithm. The set criteria are as follows:  $UDI > 75\%$ ,  $QV > 70\%$ ,  $BSR > 200$  KWh, and  $PVG > 200$  KWh. After 500 generations of optimization iterations, the four performance objectives gradually converge and stabilize. The last generation of the Pareto front solution set was selected, and duplicate data were deleted, resulting in 136 groups of valid Pareto front solution sets. Visual decision-making for the Pareto front solution sets was conducted through the Design Explorer2 platform. The parallel coordinates plot in Figure 8 displays 136 groups of Pareto front solutions, with each line segment representing a solution. The parallel coordinate plots reveal the distribution range of the four performance optimization objectives. Specifically, the UDI distribution ranges from  $75.14\%$  to  $86.30\%$ , the QV distribution ranges from  $70.04\%$  to  $82.59\%$ , and the BSR distribution ranges from  $203.60$  to  $549.80$  KWh. The PVG distribution spans from  $300.00$  to  $599.00$  KWh.

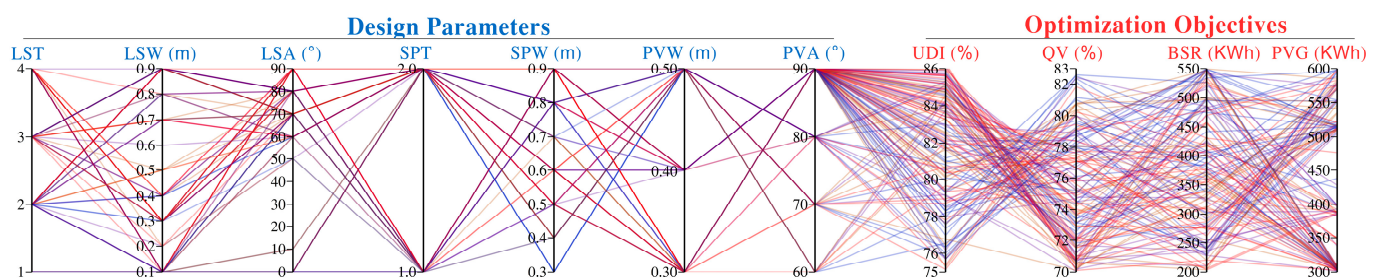


Figure 8. Parallel coordinate plots of Pareto front solutions.



Figure 9 illustrates the results of the adaptive façade design parameter distribution for the Pareto front solution. In the upper part of the adaptive façade, the light shelf module units are predominantly of types II, IV, and III. The widths of the light shelf are mainly distributed at 0.1 m, 0.9 m, and 0.3 m, with rotation angles primarily at 70°, 80°, and 0°. In the middle part of the adaptive façade, the shading module units primarily comprise the comprehensive and horizontal shading types. The widths of the shading plates are mainly distributed at 0.9 m, 0.6 m, and 0.8 m. In the lower part of the adaptive façade, the width of photovoltaic shading module units is mainly distributed at 0.5 m, 0.3 m, and 0.4 m. Additionally, the rotation angle of photovoltaic panels is mainly 90°, 80°, and 70°.

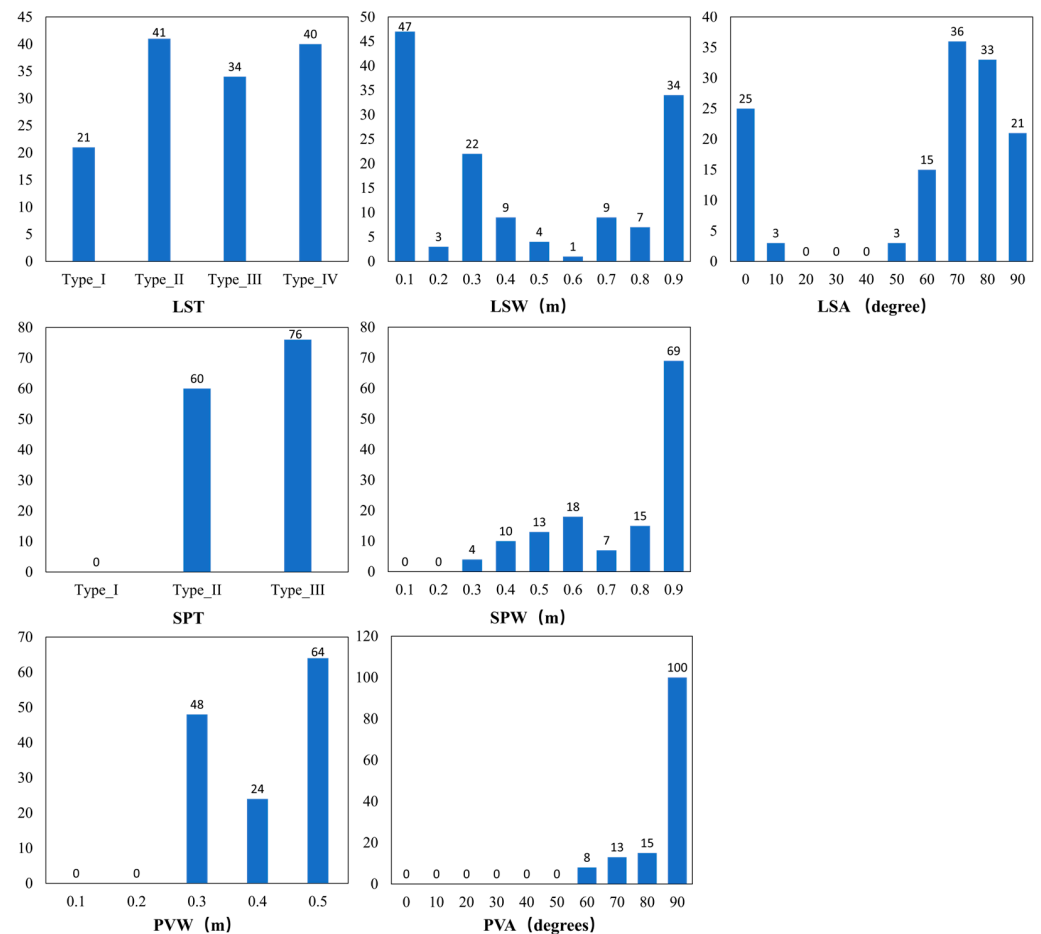


Figure 9. Design parameter distributions of the Pareto front solutions.

## 5. Discussion

Previous studies often selected traditional blinds as building envelope shading devices to regulate indoor daylighting and reduce solar heat radiation [84]. Therefore, traditional blinds were selected for the comparative analysis in this study. In the same situation, the traditional blinds are attached to an office unit, with the blind slats set at a width of 0.3 m and a spacing of 0.25 m, tilted downward at 5 degrees. As traditional blinds typically cover the entire surface of the building envelope, and using photovoltaic panels is less common, the three primary performance objectives considered were UDI, QV, and BSR. Simulations of the performance of the applied traditional blinds indicate a UDI of 85.78%, a QV of 71.43%, and a BSR of 338.69 KWh.

Considering the inherent error in the neural network prediction model and referring to traditional blinds' performance data, the decision-making screening criteria were set as follows: UDI > 84.5%, QV > 72%, and BSR > 340 KWh. Figure 10 shows the screening results from the Design Explorer platform, totaling ten groups of Pareto front solutions,

and the data are corrected by performance simulation with the specific parameters shown in Table 7. Three groups of solutions, namely Group A, Group B, and Group C demonstrate superiority over traditional blinds in all three performance aspects—UDI, QV, and BSR. Subsequently, the three groups of optimal solutions will be discussed in terms of each of the four performance aspects: UDI, QV, BSR, and PVG.

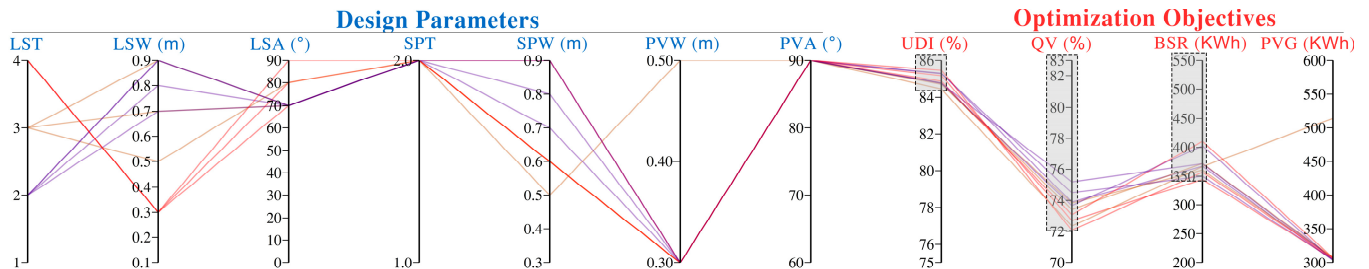


Figure 10. Standards-compliant Pareto front solutions.

Table 7. The final selected ten groups of optimal Pareto front solutions.

Group	LST	LSW (m)	LSA (°)	SPT	SPW (m)	PVW (m)	PVA (°)	UDI (%)	QV (%)	BSR (KWh)	PVG (KWh)
A	2	0.8	70	2	0.9	0.3	90	85.94	76.79	343.55	309.94
B	4	0.3	70	2	0.9	0.3	90	86.97	75.60	346.95	309.94
C	3	0.7	70	2	0.6	0.3	90	86.30	76.79	389.25	309.94
D	3	0.9	70	2	0.5	0.5	90	86.73	76.20	298.83	516.57
E	4	0.3	80	2	0.6	0.3	90	85.88	74.41	319.66	309.94
F	3	0.5	80	2	0.6	0.3	90	85.80	74.41	323.26	309.94
G	2	0.9	70	2	0.7	0.3	90	84.73	77.98	372.06	309.94
H	2	0.9	70	2	0.8	0.3	90	85.62	77.38	341.36	309.94
I	2	0.7	70	2	0.9	0.3	90	85.43	76.79	383.32	309.94
J	4	0.3	90	2	0.6	0.3	90	86.73	68.46	252.20	309.94

Section 4 shows that LSW and SPW have more significant impacts on indoor daylighting performance than other design parameters, with the same SPW parameter for both the Group A and Group B solutions. Therefore, to better analyze the indoor daylighting performance for each group of solutions, the indoor daylighting distribution maps for each group of solutions were simulated separately for three conditions: below 100 Lux (insufficient daylight), 100–2000 Lux (useful daylight), and over 2000 Lux (excessive daylight). The simulation results are shown in Figure 11.

Firstly, the daylighting performance of Group A and Group B solutions was analyzed. When comparing indoor daylighting situations with UDI (<100 Lux), the Group A solution showed a 0.28% reduction in the illumination ratio of daylight insufficiency compared to the Group B solution. Conversely, when comparing UDI (>2000 Lux), it was observed that the Group A solution had a 1.24% increase in UDI compared to the Group B solution, resulting in a 1.04% reduction in useful indoor daylighting illuminance in the Group A solution. The reason for that difference is that the module units on the upper part of the adaptive façade in the Group A solution incorporate two light shelf panels, each with a width of 0.8 m and spaced at 0.5 m intervals. This configuration allows more outdoor sunlight to enter the room through reflection, thereby increasing the overall daylighting illuminance of the room. Consequently, the proportion of sunlight exceeding 2000 Lux increases, while the proportion of UDI between 100 and 2000 Lux decreases. In contrast, the upper module units of the adaptive façade in the Group B solution comprise four 0.3 m wide light shelf panels arranged at a spacing of 0.15 m. With a narrower LSW of 0.3 m, sunlight entering the room through reflection is reduced. This design avoids excessive indoor daylighting illuminance while increasing the indoor daylighting illuminance ratio to meet the requirements of 100–2000 Lux.

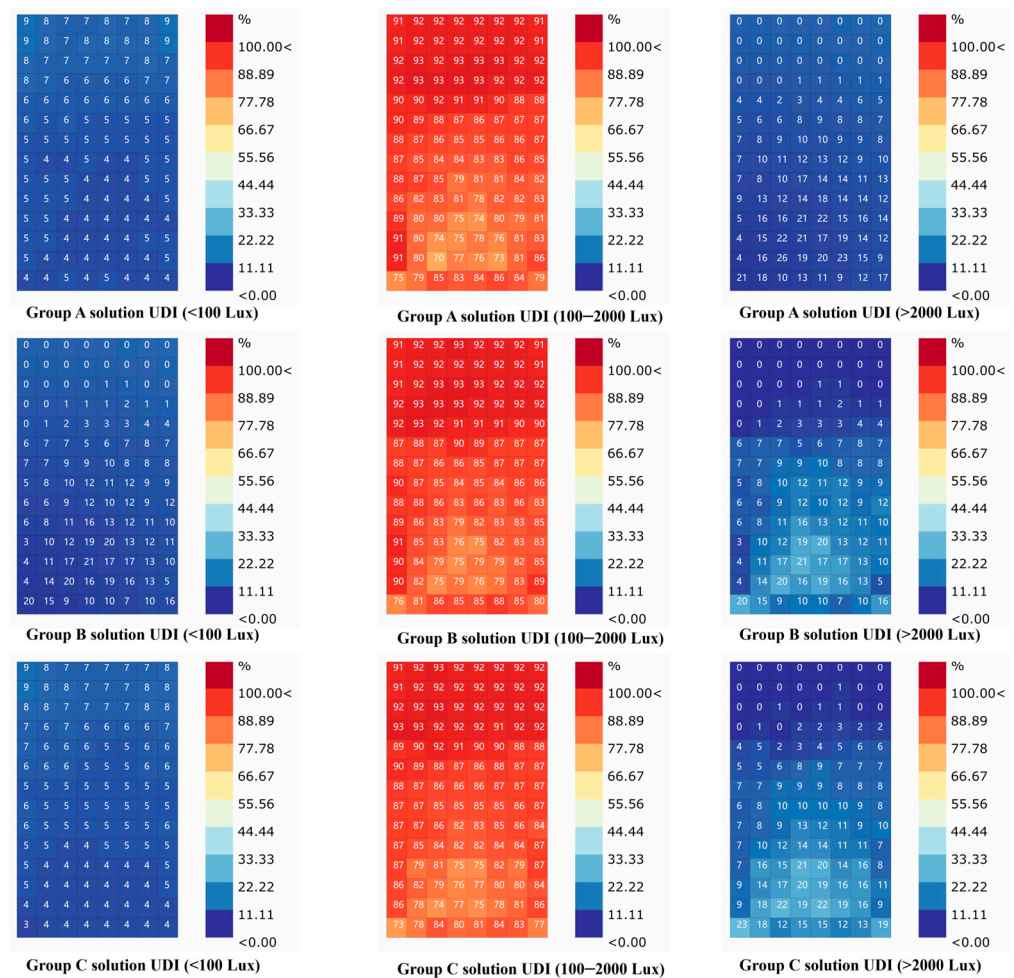


Figure 11. Indoor daylight distributions for the three groups of solutions.

Additionally, the Group C solution differs in the adaptive façade design parameters LST, LSW, and SPW compared to the Group A and B solutions. The Group C solution consists of three light shelf planes with a width of 0.7 m, spaced at 0.25 m intervals. The 0.7 m width of the light shelf allows more outdoor sunlight to enter the room through reflection, thereby improving indoor daylighting in deeper spaces. However, utilizing comprehensive shading with a width of 0.6 m in the adaptive façade diminishes the shading effect on outdoor sunlight. Consequently, there is an increase in the proportion of illuminance over 2000 Lux at the daylighting test points in the near-window section. In summary, Group B solutions have the best indoor daylighting performance, followed by Group C solutions, while Group A solutions are relatively poor.

Secondly, concerning the indoor view performance analysis, as discussed in Section 4, the Pearson correlation coefficient reveals that PVA has the most significant impact on the QV compared to other adaptive façade design parameters. It is worth mentioning that PVA is set at 90° for all three solution groups. As shown in Table 7, the indoor view performance for the Group A solution is equal to that of the Group C solution, and both surpass the QV achieved by the Group B solution ( $QV_A = QV_C > QV_B$ ). All three solution groups meet the LEED v4 requirement, ensuring that at least 75% of the regularly occupied floor area provides outside views.

Figure 12 illustrates a more detailed analysis of these three groups' indoor view performance. This study selected a view factor of five as the evaluation criterion in the indoor view performance simulation. It was found that the test areas of Group A solutions and Group C solutions with a view factor of more than five were almost the same. Therefore, the QV for Group A solutions is equal to that of Group C solutions. However, Figure 12

shows that the test area with a view factor of more than 15 for the Group C solution is significantly larger than that for the Group A and B solutions in the near-window section of the office. Furthermore, the SPW of the adaptive façade design parameter negatively correlates with the QV. The 0.6 m width of the shading plate for the Group C solution is smaller than the 0.9 m width of the shading plate for the Group A and Group B solutions, contributing to the superior QV in the Group C solution when compared to the Group A and Group B solutions.

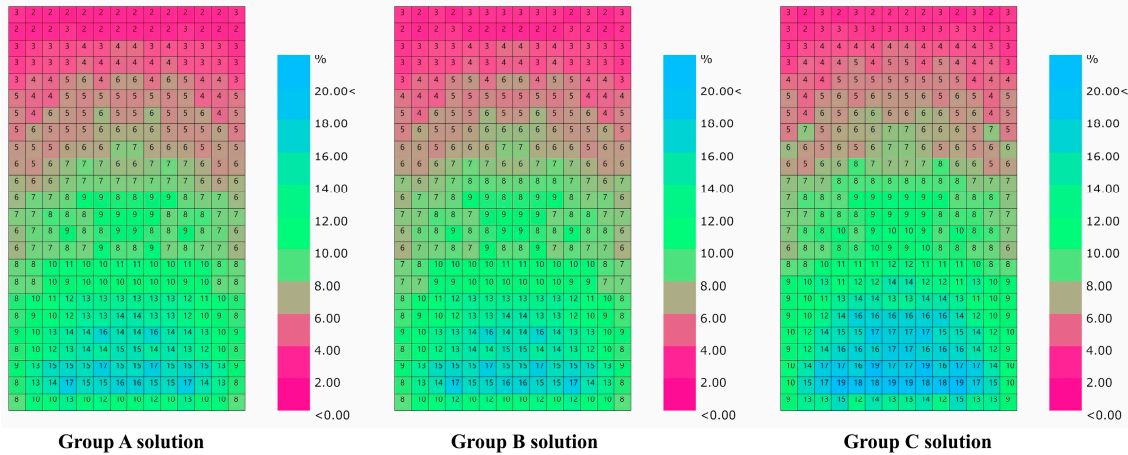


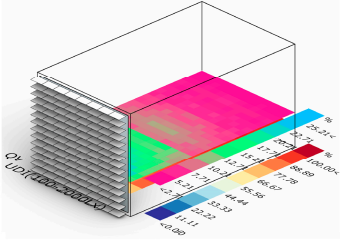
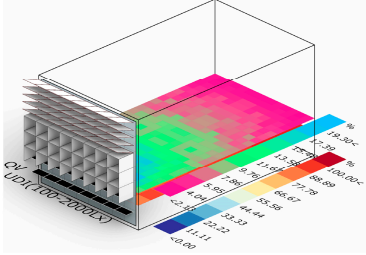
**Figure 12.** Distribution of the QV for the three groups of solutions.

Regarding the analysis of BSR, the BSR of the Group C solution is significantly better than that of the Group B and Group A solutions in Table 7. According to the correlation coefficient analysis in Section 4, SPW and PVA have more significant impacts on the BSR than other design parameters and show negative correlations. The design parameter PVA for the three groups of solutions is 0.3 m. Therefore, the influence of SPW parameters on BSR is primarily analyzed. The SPW of 0.6 m for the Group C solution is smaller than that of 0.9 m for the Group A and Group B solutions. The SPW of the group C solution allows more beneficial winter solar radiation energy to be projected onto the building envelope, thereby improving indoor temperatures.

Finally, according to the solar photovoltaic power generation analysis based on the correlation coefficient analysis in Section 4, the parameter PVW has a strong positive correlation with PVG. Since all three solutions of PV panels have a width of 0.3 m and the same rotation angle of  $90^\circ$ , the PVG of each group of solutions is 309.94 KWh.

In summary, although Group C's solution is weaker than Group B's regarding indoor daylighting performance, it is better than Group A's and Group B's solutions regarding indoor view performance and beneficial solar radiation energy performance. Therefore, the Group C solution was selected to compare the building performance analysis with the traditional blinds. Table 8 indicates that the adaptive façade corresponding to the Group C solution outperforms traditional blinds in all building performance indicators. Notably, the most significant improvement is observed in the performance of beneficial solar radiation energy, with an increase of 51.26 KWh, representing a 14.93% improvement. Secondly, there is a 5.36% enhancement of indoor view performance. The indoor daylighting performance improved by 0.52%. Additionally, using photovoltaic shading systems resulted in 309.9 KWh of solar photovoltaic power per office unit per year.

**Table 8.** Building performance of traditional blinds versus adaptive façades.

		UDI (%)	QV (%)	BSR (KWh)	PVG (KWh)
Traditional blinds		85.78	71.43	338.69	/
Adaptive façade		86.30	76.79	389.25	309.94
Enhancement		0.52	5.36	51.56	309.94

## 6. Conclusions

This research proposes an adaptive façade optimization design framework integrating a 3D parametric model, performance models, neural network prediction models, multi-objective optimization, and decision-making. It selects a typical office building in Jinan City as a study case for practical application. Reviewing the previous research results of the adaptive façade design process and applying optimization algorithms and artificial intelligence technology in the building adaptive façade design field provide essential technical support and reference for the study. Finally, the optimized adaptive façade was compared with traditional blinds. The results indicate that the adaptive façade design, based on building envelope performance characteristics, has excellent performance in multiple aspects of building performance. The novelty and originality of the whole study are presented in two aspects. Firstly, the framework integrates four building performance objectives: UDI, QV, BSR, and PVG. It achieves a quickly optimized design of the building's adaptive façade by combining a neural network prediction model with a multi-objective optimization algorithm. Secondly, through the K-means clustering algorithm, the performance characteristics of the building envelope are fully explored to establish a functional connection between the building envelope and the adaptive façade design, providing data support for the optimization design of the adaptive façade.

The primary outcomes of the study are as follows:

1. The research framework uses a parametric platform that integrates performance simulation, clustering analysis, a neural network prediction model, and multi-objective optimization decision-making, establishing an integrated framework for adaptive façade optimization design and improving the efficiency of adaptive façade design.
2. The functional connection between building envelope performance characteristics and adaptive façade design was explored. Through a K-means clustering analysis of the performance characteristics of the building envelope, it is divided into three parts with different functional attributes: the upper part mainly corresponds to the daylighting performance, the middle part corresponds to the view and daylighting performance, and the lower part mainly corresponds to the view and solar radiation heat gain performance. This division provides data support for the targeted design of the adaptive façade.

3. The research reveals the interactions between four building performance objectives (UDI, QV, BSR, and PVG) and adaptive façade design parameters of the office building in this case through Pearson's correlation coefficient analysis, where LSW and SPW have significant impacts on UDI, PVA on QV, SPW on BSR, and PVW on PVG.
4. The research focuses on optimizing the design of building adaptive façades from three aspects: indoor daylighting performance, view performance, and solar energy utilization. Compared with traditional blinds, the UDI, QV, and BSR performance indicators have improved by 0.52%, 5.36%, and 14.93%, respectively. Additionally, using photovoltaic shading technology can also generate 309.94 KWh of photovoltaic power.

This study presents some limitations. Firstly, this study used only BPNN as a building performance prediction model. Attempts at using other machine learning methods, such as the random forest model [85], the support vector machine model, and the decision tree model, should be tried. The building performance prediction effect can be evaluated more comprehensively by comparing the prediction accuracy of different machine learning methods. Secondly, the study only used simulated data. It did not use actual measured data for analysis and calibration, which may lead to some deviation of the research results from the actual situation. In order to improve the accuracy and reliability of the study, it is recommended that simulated data be corrected using actual measurement data in future studies [86]. Finally, the application case for this study is an office building in northern China. Considering that the optimal inclination of blind slats is affected by geographical latitude [87], the impact of adaptive façades on indoor performance may vary in different climatic regions. In order to fully validate the applicability of this design framework, it is recommended that climate zones at different latitudes be selected for experimentation and validation in future studies [88].

Future research can combine the specific behavioral state of indoor users; take advantage of parametric modeling, performance simulation, artificial intelligence, and other advanced technologies for solving complex scientific problems; and design adaptive façades for human–computer interaction. Secondly, to meet the aesthetic demand, it is necessary to design a uniformly changing adaptive façade that can respond to different functional attributes of the building envelope, adjust the corresponding adaptive façade morphology, and even form the required pattern according to the state of the building envelope. In addition, we will further explore and improve the interdisciplinary integration of mechanical engineering, control science and engineering, computer science, and electrical engineering in the adaptive facade operating system in order to achieve a more efficient and intelligent adaptive facade.

**Author Contributions:** Conceptualization, P.C.; methodology, P.C.; software, H.T.; validation, H.T.; formal analysis, H.T.; investigation, H.T.; resources, H.T.; data curation, H.T.; writing—original draft preparation, H.T.; writing—review and editing, P.C.; visualization, H.T.; supervision, P.C.; project administration, P.C.; funding acquisition, P.C. All authors have read and agreed to the published version of the manuscript.

**Funding:** This research was funded by the Shandong Provincial Fund of Key Advantageous Discipline (Architecture) and the Natural Science Foundation of Shandong Province (No. ZR2021ME133).

**Data Availability Statement:** Data are available upon reasonable request.

**Acknowledgments:** The authors thank the anonymous reviewers for their comments on this manuscript.

**Conflicts of Interest:** The authors declare no conflicts of interest.

## References

1. Ahmed, A.; Ge, T.; Peng, J.; Yan, W.C.; Tee, B.T.; You, S. Assessment of the renewable energy generation towards net-zero energy buildings: A review. *Energy Build.* **2022**, *256*, 111755. [[CrossRef](#)]
2. Aldossary, N.A.; Rezgui, Y.; Kwan, A. Establishing domestic low energy consumption reference levels for Saudi Arabia and the Wider Middle Eastern Region. *Sustain. Cities Soc.* **2017**, *28*, 265–276. [[CrossRef](#)]

3. Holechek, J.L.; Geli, H.M.; Sawalhah, M.N.; Valdez, R. A global assessment: Can renewable energy replace fossil fuels by 2050? *Sustainability* **2022**, *14*, 4792. [CrossRef]
4. Li, J.; Zhang, C.; Zhao, Y.; Qiu, W.; Chen, Q.; Zhang, X. Federated learning-based short-term building energy consumption prediction method for solving the data silos problem. In *Building Simulation*; Tsinghua University Press: Beijing, China, 2022; Volume 15, pp. 1145–1159. [CrossRef]
5. Kumar, G.; Raheja, G. Design determinants of building envelope for sustainable built environment: A review. *Int. J. Built Environ. Sustain.* **2016**, *3*. [CrossRef]
6. Nasrollahzadeh, N. Comprehensive building envelope optimization: Improving energy, daylight, and thermal comfort performance of the dwelling unit. *J. Build. Eng.* **2021**, *44*, 103418. [CrossRef]
7. Pollution, I.A. *Report to Congress on Indoor Air Quality*; EPA/400/1; Environmental Protection Agency Office of Research and Development: Washington, DC, USA, 1989. Available online: [https://www.aivc.org/sites/default/files/airbase\\_4294.pdf](https://www.aivc.org/sites/default/files/airbase_4294.pdf) (accessed on 23 April 2024).
8. Ghodrati, N.; Samari, M.; Shafiei, M.W.M. Green buildings impacts on occupants' health and productivity. *J. Appl. Sci. Res.* **2012**, *8*, 4235–4241.
9. Chen, Y.; Li, M.; Lu, J.; Chen, B. Influence of residential indoor environment on quality of life in China. *Build. Environ.* **2023**, *232*, 110068. [CrossRef]
10. Mangkuto, R.A.; Dewi, D.K.; Herwandani, A.A.; Koerniawan, M.D. Design optimization of internal shading device in multiple scenarios: Case study in Bandung, Indonesia. *J. Build. Eng.* **2019**, *24*, 100745. [CrossRef]
11. Barozzi, M.; Lienhard, J.; Zanelli, A.; Monticelli, C. The sustainability of adaptive envelopes: Developments of kinetic architecture. *Procedia Eng.* **2016**, *155*, 275–284. [CrossRef]
12. Brown, T.M.; Brainard, G.C.; Cajochen, C.; Czeisler, C.A.; Hanifin, J.P.; Lockley, S.W.; Lucas, R.J.; Münch, M.; O'Hagan, J.B.; Peirson, S.N.; et al. Recommendations for daytime, evening, and nighttime indoor light exposure to best support physiology, sleep, and wakefulness in healthy adults. *PLoS Biol.* **2022**, *20*, e3001571. [CrossRef]
13. Cheng, C.L.; Chen, C.L.; Chou, C.P.; Chan, C.Y. A mini-scale modeling approach to natural daylight utilization in building design. *Build. Environ.* **2007**, *42*, 372–384. [CrossRef]
14. Lim, Y.-W.; Ahmad, M.H.; Ossen, D.R. Internal shading for efficient tropical daylighting in Malaysian contemporary high-rise open plan office. *Indoor Built Environ.* **2013**, *22*, 932–951. [CrossRef]
15. Reinhart, C.F. *Daylighting Handbook II. Daylight Simulations and Dynamic Façades*; Building Technology Press: Cambridge, MA, USA, 2018.
16. Konis, K. A novel circadian daylight metric for building design and evaluation. *Build. Environ.* **2017**, *113*, 22–38. [CrossRef]
17. Abd-Alhamid, F.; Kent, M.; Wu, Y. Quantifying window view quality: A review on view perception assessment and representation methods. *Build. Environ.* **2022**, *227*, 109742. [CrossRef]
18. Pilechiha, P.; Mahdavinejad, M.; Rahimian, F.P.; Carnemolla, P.; Seyedzadeh, S. Multi-objective optimization framework for designing office windows: Quality of view, daylight and energy efficiency. *Appl. Energy* **2020**, *261*, 114356. [CrossRef]
19. Knecht, C. Urban nature and well-being: Some empirical support and design implications. *Berkeley Plan. J.* **2004**, *17*. [CrossRef]
20. Heerwagen, J.H.; Orians, G.H. Adaptations to Window lessness: A study of the use of visual decor in windowed and windowless offices. *Environ. Behav.* **1986**, *18*, 623–639. [CrossRef]
21. Aries, M.B.C.; Veitch, J.A.; Newsham, G.R. Physical and psychological discomfort in the office environment. In Proceedings of the Light, Performance and Quality of Life—Light and Health Research Foundation (SOLG) Symposium, Eindhoven, The Netherlands, 8 November 2007; pp. 45–50.
22. Hescong, L.; Mahone, D. *Windows and Offices: A Study of Office Worker Performance and the Indoor Environment*; California Energy Commission: California, CA, USA, 2003; pp. 1–5.
23. Kent, M.; Parkinson, T.; Kim, J.; Schiavon, S. A data-driven analysis of occupant workspace dissatisfaction. *Build. Environ.* **2021**, *205*, 108270. [CrossRef]
24. Andersen, M. Unweaving the human response in daylighting design. *Build. Environ.* **2015**, *91*, 101–117. [CrossRef]
25. *Technical Committee CEN/TC 169, EN 17037:2018 Daylight in Buildings*; European Committee for Standardization CEN-CENELEC: Brussels, Belgium, 2018.
26. Pouyanmehr, M.; Pilechiha, P.; Berardi, U.; Carnemolla, P. External shading form-finding: Simulating daylighting and dynamic view access assessment. *J. Build. Perform. Simul.* **2022**, *15*, 398–409. [CrossRef]
27. Kumar, D.S.; Yagli, G.M.; Kashyap, M.; Srinivasan, D. Solar irradiance resource and forecasting: A comprehensive review. *IET Renew. Power Gener.* **2020**, *14*, 1641–1656. [CrossRef]
28. Li, R.; Satchwell, A.J.; Finn, D.; Christensen, T.H.; Kummert, M.; Le Dréau, J.; Lopes, R.A.; Madsen, H.; Salom, J.; Henze, G.; et al. Ten questions concerning energy flexibility in buildings. *Build. Environ.* **2022**, *223*, 109461. [CrossRef]
29. Qian, S.; Long, E.; Guo, S.; Zhang, Y.; Zhao, Y. Study on the influence of different surface colors on energy consumption of mall in hot summer and cold winter areas. *IOP Conf. Ser. Earth Environ. Sci.* **2020**, *463*, 12029. [CrossRef]
30. Kuhn, T.E.; Erban, C.; Heinrich, M.; Eisenlohr, J.; Ensslen, F.; Neuhaus, D.H. Review of technological design options for building integrated photovoltaics (BIPV). *Energy Build.* **2021**, *231*, 110381. [CrossRef]
31. Ghosh, A. Potential of building integrated and attached/applied photovoltaic (BIPV/BAPV) for adaptive less energy-hungry building's skin: A comprehensive review. *J. Clean. Prod.* **2020**, *276*, 123343. [CrossRef]

32. Yadav, S.; Panda, S.K. Thermal performance of BIPV system by considering periodic nature of insolation and optimum tilt-angle of PV panel. *Renew. Energy* **2020**, *150*, 136–146. [[CrossRef](#)]
33. Tabasi, S.F.; Banihashemi, S. Design and mechanism of building responsive skins: State-of-the-art and systematic analysis. *Front. Archit. Res.* **2022**, *11*, 1151–1176. [[CrossRef](#)]
34. Liu, X.; Shen, C.; Wang, J.; Zhang, C.; Shuai, Y. Static and dynamic regulations of photovoltaic double skin facades towards building sustainability: A review. *Renew. Sustain. Energy Rev.* **2023**, *183*, 113458. [[CrossRef](#)]
35. Loonen, R.C.; Trčka, M.; Cóstola, D.; Hensen, J.L. Climate adaptive building shells: State-of-the-art and future challenges. *Renew. Sustain. Energy Reviews.* **2013**, *25*, 483–493. [[CrossRef](#)]
36. Tabadkani, A.; Roetzel, A.; Li, H.X.; Tsangrassoulis, A. Design approaches and typologies of adaptive facades: A review. *Autom. Constr.* **2021**, *121*, 103450. [[CrossRef](#)]
37. Chamilothori, K.; Chinazzo, G.; Rodrigues, J.; Dan-Glauser, E.S.; Wienold, J.; Andersen, M. Subjective and physiological responses to façade and sunlight pattern geometry in virtual reality. *Build. Environ.* **2019**, *150*, 144–155. [[CrossRef](#)]
38. Van Den Wymelenberg, K. Patterns of occupant interaction with window blinds: A literature review. *Energy Build.* **2012**, *51*, 165–176. [[CrossRef](#)]
39. Olbina, S.; Hu, J. Daylighting and thermal performance of automated split-controlled blinds. *Build. Environ.* **2012**, *56*, 127–138. [[CrossRef](#)]
40. Alsukkar, M.; Hu, M.; Eltaweel, A.; Su, Y. Daylighting performance improvements using of split louver with parametrically incremental slat angle control. *Energy Build.* **2022**, *274*, 112444. [[CrossRef](#)]
41. Alsukkar, M.; Hu, M.; Gadi, M.; Su, Y. A study on daylighting performance of split louver with simplified parametric control. *Buildings* **2022**, *12*, 594. [[CrossRef](#)]
42. Kim, J.T.; Kim, G. Advanced external shading device to maximize visual and view performance. *Indoor Built Environ.* **2010**, *19*, 65–72. [[CrossRef](#)]
43. Valitabar, M.; Ghaffarian, H.A.; Attia, S. Advanced control strategy to maximize view and control discomforting glare: A complex adaptive façade. *Archit. Eng. Des. Manag.* **2022**, *18*, 829–849. [[CrossRef](#)]
44. Touloupaki, E.; Theodosiou, T. Performance simulation integrated in parametric 3D modeling as a method for early stage design optimization—A review. *Energies* **2017**, *10*, 637. [[CrossRef](#)]
45. Kim, H.; Clayton, M.J. A multi-objective optimization approach for climate-adaptive building envelope design using parametric behavior maps. *Build. Environ.* **2020**, *185*, 107292. [[CrossRef](#)]
46. Kim, H.; Clayton, M.J. Parametric behavior maps: A method for evaluating the energy performance of climate-adaptive building envelopes. *Energy Build.* **2020**, *219*, 110020. [[CrossRef](#)]
47. Wu, H.; Zhang, T. Optimal design of complex dynamic shadings: Towards sustainable built environment. *Sustain. Cities Soc.* **2022**, *86*, 104109. [[CrossRef](#)]
48. Samadi, S.; Noorzai, E.; Beltrán, L.O.; Abbasi, S. A computational approach for achieving optimum daylight inside buildings through automated kinetic shading systems. *Front. Archit. Res.* **2020**, *9*, 335–349. [[CrossRef](#)]
49. Wang, S.; Zhang, Q.; Liu, P.; Liang, R.; Fu, Z. A Parameterized design method for building a shading system based on climate adaptability. *Atmosphere* **2022**, *13*, 1244. [[CrossRef](#)]
50. Wang, L.; Zhang, H.; Liu, X.; Ji, G. Exploring the synergy of building massing and façade design through evolutionary optimization. *Front. Archit. Res.* **2022**, *11*, 761–780. [[CrossRef](#)]
51. Shen, L.; Han, Y. Optimizing the modular adaptive façade control strategy in open office space using integer programming and surrogate modelling. *Energy Build.* **2022**, *254*, 111546. [[CrossRef](#)]
52. Hosseini, S.M.; Mohammadi, M.; Guerra-Santin, O. Interactive kinetic façade: Improving visual comfort based on dynamic daylight and occupant's positions by 2D and 3D shape changes. *Build. Environ.* **2019**, *165*, 106396. [[CrossRef](#)]
53. Hosseini, S.M.; Mohammadi, M.; Schröder, T.; Guerra-Santin, O. Integrating interactive kinetic façade design with colored glass to improve daylight performance based on occupants' position. *J. Build. Eng.* **2020**, *31*, 101404. [[CrossRef](#)]
54. Rizi, R.A.; Eltaweel, A. A user detective adaptive facade towards improving visual and thermal comfort. *J. Build. Eng.* **2021**, *33*, 101554. [[CrossRef](#)]
55. Yussuf, R.O.; Asfour, O.S. Applications of artificial intelligence for energy efficiency throughout the building lifecycle: An overview. *Energy Build.* **2024**, *305*, 113903. [[CrossRef](#)]
56. Datta, S.D.; Islam, M.; Sobuz, M.H.R.; Ahmed, S.; Kar, M. Artificial intelligence and machine learning applications in the project lifecycle of the construction industry: A comprehensive review. *Heliyon* **2024**, *10*, e26888. [[CrossRef](#)]
57. Regona, M.; Yigitcanlar, T.; Hon, C.; Teo, M. Artificial intelligence and sustainable development goals: Systematic literature review of the construction industry. *Sustain. Cities Soc.* **2024**, *108*, 105499. [[CrossRef](#)]
58. Hu, J.; Olbina, S. Illuminance-based slat angle selection model for automated control of split blinds. *Build. Environ.* **2011**, *46*, 786–796. [[CrossRef](#)]
59. Gadelhak, M. Integrating computational and building performance simulation techniques for optimized facade designs. In *eCAADe 2013: Computation and Performance—Proceedings of the 31st International Conference on Education and Research in Computer Aided Architectural Design in Europe, Delft, The Netherlands, 18–20 September 2013*; Faculty of Architecture, Delft University of Technology: Delft, The Netherlands; eCAADe (Education and research in Computer Aided Architectural Design in Europe): Nicosia, Cyprus, 2013. [[CrossRef](#)]



60. Sadegh, S.O.; Gasparri, E.; Brambilla, A.; Globa, A. Kinetic facades: An evolutionary-based performance evaluation framework. *J. Build. Eng.* **2022**, *53*, 104408. [[CrossRef](#)]
61. Luo, Z.; Sun, C.; Dong, Q. A daylight-linked shading strategy for automated blinds based on model-based control and Radial Basis Function (RBF) optimization. *Build. Environ.* **2020**, *177*, 106854. [[CrossRef](#)]
62. Lin, C.-H.; Tsay, Y.-S. A metamodel based on intermediary features for daylight performance prediction of facade design. *Build. Environ.* **2021**, *206*, 108371. [[CrossRef](#)]
63. El-Mowafy, B.N.; Elmokadem, A.A.; Waseef, A.A. Evaluating adaptive facade performance in early building design stage: An integrated daylighting simulation and machine learning. In Proceedings of the 8th International Conference on Advanced Machine Learning and Technologies and Applications (AMLT2022), Cairo, Egypt, 5–7 2022; Springer International Publishing: Cham, Switzerland, 2022; pp. 211–223. [[CrossRef](#)]
64. Li, Y.; Huang, C.; Zhang, G.; Yao, J. Machine learning modeling and genetic optimization of adaptive building facade towards the light environment. In Proceedings of the 27th International Conference of the Association for ComputerAided Architectural Design Research in Asia (CAADRIA), Tokyo, Japan, 22–29 March 2025; pp. 141–150. [[CrossRef](#)]
65. Alsharif, R.; Arashpour, M.; Golafshani, E.; Rashidi, A.; Li, H. Multi-objective optimization of shading devices using ensemble machine learning and orthogonal design of experiments. *Energy Build.* **2023**, *283*, 112840. [[CrossRef](#)]
66. McNeel, R. Grasshopper-algorithmic modeling for Rhino. Available online: <http://www.grasshopper3d.com> (accessed on 23 April 2024).
67. Zhang, J.; Liu, S.; Han, J.; Zhou, L.; Liu, Y.; Yang, L.; Zhang, J.; Zhang, Y. Impact of heat waves on nonaccidental deaths in Jinan, China, and associated risk factors. *Int. J. Biometeorol.* **2016**, *60*, 1367–1375. [[CrossRef](#)]
68. Roudsari, M.S.; Pak, M. Ladybug: A parametric environmental plugin for grasshopper to help design. In *Building Simulation; IBPSA*: London, UK, 2013. Available online: <https://www.aivc.org/resource/ladybug-parametric-environmental-plugin-grasshopper-help-designers-create-environmentally> (accessed on 23 April 2024).
69. Jiang, C.; Liang, X.; Zhou, Y.C.; Tian, Y.; Xu, S.; Lin, J.R.; Ma, Z.; Yang, S.; Zhou, H. A multilayer perceptron-based fast sunlight assessment for the conceptual design of residential neighborhoods under Chinese policy. *Build. Environ.* **2023**, *244*, 110739. [[CrossRef](#)]
70. Kensek, K.; Suk, J.Y. Daylight Factor (overcast sky) versus Daylight Availability (clear sky) in Computer-based Daylighting Simulations. *J. Creat. Sustain. Archit. Built Environ.* **2011**, *1*, 3–14.
71. Li, D.; Lau, C.; Lam, J. Predicting daylight illuminance by computer simulation techniques. *Light. Res. Technol.* **2004**, *36*, 113–128. [[CrossRef](#)]
72. Nabil, A.; Mardaljevic, J. Useful daylight illuminance: A new paradigm for assessing daylight in buildings. *Light. Res. Technol.* **2005**, *37*, 41–57. [[CrossRef](#)]
73. Reinhart, C.F.; Walkenhorst, O. Validation of dynamic RADIANCE-based daylight simulations for a test office with external blinds. *Energy Build.* **2001**, *33*, 683–697. [[CrossRef](#)]
74. U.S. Green Building Council, Leadership in Energy and Environmental Design LEED V4; Volume 1. 2021. Available online: <https://new.usgbc.org/leed-v41> (accessed on 23 April 2024).
75. Zhang, L.; Zhang, L.; Wang, Y. Shape optimization of free-form buildings based on solar radiation gain and space efficiency using a multi-objective genetic algorithm in the severe cold zones of China. *Sol. Energy* **2016**, *132*, 38–50. [[CrossRef](#)]
76. Yan, H.; Yan, K.; Ji, G. Optimization and prediction in the early design stage of office buildings using genetic and XGBoost algorithms. *Build. Environ.* **2022**, *218*, 109081. [[CrossRef](#)]
77. Ikotun, A.M.; Ezugwu, A.E.; Abualigah, L.; Abuhaija, B.; Heming, J. K-means clustering algorithms: A comprehensive review, variants analysis, and advances in the era of big data. *Inf. Sci.* **2023**, *622*, 178–210. [[CrossRef](#)]
78. Kontovourkis, O.; Panayiotou, P.N. Machine learning to classify and predict design and fabrication solutions of architectural prototypes driven by sustainable criteria. In *Advances in Product Design Engineering*; Springer International Publishing: Cham, Switzerland, 2022; pp. 105–130. [[CrossRef](#)]
79. Loh, W.-L. On Latin hypercube sampling. *Ann. Stat.* **1996**, *24*, 2058–2080. [[CrossRef](#)]
80. Asadi, E.; Da Silva, M.G.; Antunes, C.H.; Dias, L.; Glicksman, L. Multi-objective optimization for building retrofit: A model using genetic algorithm and artificial neural network and an application. *Energy Build.* **2014**, *81*, 444–456. [[CrossRef](#)]
81. Natanian, J. Optimizing mixed-use district designs in hot climates: A two-phase computational workflow for energy balance and environmental performance. *Sustain. Cities Soc.* **2023**, *98*, 104800. [[CrossRef](#)]
82. Vierlinger, R.; Bollinger, K. Accommodating change in parametric design. In Proceedings of the Association for Computer Aided Design in Architecture, Los Angeles, CA, USA, 23–25 October 2014; pp. 609–618. [[CrossRef](#)]
83. Rosso, F.; Ciancio, V.; Dell’Olmo, J.; Salata, F. Multi-objective optimization of building retrofit in the Mediterranean climate by means of genetic algorithm application. *Energy Build.* **2020**, *216*, 109945. [[CrossRef](#)]
84. Rafati, N.; Hazbei, M.; Eicker, U. Louver configuration comparison in three Canadian cities utilizing NSGA-II. *Build. Environ.* **2023**, *229*, 109939. [[CrossRef](#)]
85. Vahdatikhaki, F.; Barus, M.V.; Shen, Q.; Voordijk, H.; Hammad, A. Hammad, Surrogate modelling of solar radiation potential for the design of PV module layout on entire façade of tall buildings. *Energy Build.* **2023**, *286*, 112958. [[CrossRef](#)]
86. De Luca, F.; Sepúlveda, A.; Varjas, T. Multi-performance optimization of static shading devices for glare, daylight, view and energy consideration. *Build. Environ.* **2022**, *217*, 109110. [[CrossRef](#)]

87. Palmero-Marrero, A.I.; Oliveira, A.C. Effect of louver shading devices on building energy requirements. *Appl. Energy* **2010**, *87*, 2040–2049. [[CrossRef](#)]
88. Shafavi, S.N.S.; Dehnavi, A.N.; Zomorodian, Z.S.; Tahsildoost, M.; Korsavi, S.S.; Mohaghegh, S. Façade design of side-lit spaces for different climates and surroundings by machine learning and NSGAIII. *Build. Environ.* **2023**, *245*, 110851. [[CrossRef](#)]

**Disclaimer/Publisher’s Note:** The statements, opinions and data contained in all publications are solely those of the individual author(s) and contributor(s) and not of MDPI and/or the editor(s). MDPI and/or the editor(s) disclaim responsibility for any injury to people or property resulting from any ideas, methods, instructions or products referred to in the content.